Interfacial Communications in Recombinant Rabbit Kidney Pyruvate Kinase[†,‡]

Robert H. E. Friesen,[§] Anita J. Chin, David W. Ledman, and J. Ching Lee*

Department of Human Biological Chemistry and Genetics, The University of Texas Medical Branch at Galveston, Galveston, Texas 77555-1055

Received August 12, 1997; Revised Manuscript Received December 3, 1997

ABSTRACT: Tissue-specific isozymes of pyruvate kinase are particularly attractive systems to elucidate the molecular mechanism(s) of conferring allostery. The muscle- and kidney-type isozymes are coded by the same gene. As a consequence of alternative message RNA splicing, the two primary sequences differ by a small number of residues. However, they exhibit very different regulatory behavior. In an effort to identify the roles of specific residues in conferring allostery, the gene encoding rabbit kidney-type pyruvate kinase was cloned and expressed in *Escherichia coli*. The primary structure of recombinant rabbit kidney-type pyruvate kinase (rRKPK) and recombinant rabbit muscle-type pyruvate kinase (rRMPK) differ at 22 positions, which are located in a region that forms important intersubunit contacts in the RMPK structure. Velocity sedimentation and analytical gel chromatographic studies show that rRKPK undergoes reversible dimer ↔ tetramer assembly with an equilibrium constant of 28 ± 3 mL/mg. This subunit assembly process provides the opportunity to elucidate the role of this dimer interface in transmission of signal upon binding of substrates and allosteric effectors. The assembly to tetrameric rRKPK is favored by the binding of phosphoenolpyruvate (PEP), one of the two substrates, or fructose 1,6-bisphosphate (FBP), an activator. In contrast, the equilibrium is shifted toward dimeric rRKPK upon binding of adenosine diphosphate (ADP), the other substrate, or L-phenylalanine (Phe), the inhibitor. These observations provide significant new insights to the molecular mechanism of allosteric regulation in the pyruvate kinase system. First, all substrates and effectors communicate through this particular dimer−dimer interface. Second, the thermodynamic signatures of these communications are qualitatively different for the two substrates and between the activator, FBP, and inhibitor, Phe.

One central feature in allosteric regulation is site−site interaction between various effector binding sites (*1*−*3*). An obvious implication of site−site interaction is the presence of long-range communication via various structural elements of the protein and interfacial interactions between subunits, as essentially all allosteric systems are multisubunit proteins. An elucidation of the molecular mechanism of allosteric regulation will have to address the issues of long-range communication by defining the pathways of communication. A powerful approach is to define the thermodynamic signature of communication associated with each specific effector. Thus, there is no better approach to probe intersubunit communication than to monitor the effects of ligands on the energetics of subunit assembly. However, in those allosteric systems that consist of stable complexes of multisubunits, it is virtually impossible to identify the pathway of communication via specific intersubunit interface since rarely are there probes strategically placed among the different intersubunit interfaces to report the changes in these interfaces in response to the binding of effectors. In contrast, any allosteric system that undergoes subunit assembly has a distinct advantage as a subject of investigation of pathway of communication since one may monitor with precision the effects of ligand binding on the energetics of subunit assembly. A judicious application of this approach can ultimately lead to an establishment of the ground rules of allosteric regulation.

Mammalian pyruvate kinase (PK),[1] a key regulatory glycolytic enzyme, exhibits some properties to establish it as an ideal subject of investigation to elucidate the molecular mechanism of allosteric regulation.

(A) In vertebrates, PK is expressed in isozymic forms in a tissue-specific manner (*4*). The muscle-type PK is the major isozyme in cardiac muscle and brain and is the only isozyme found in adult skeletal muscle. The kidney-type

[†] Supported by Grants H-0013 and H-1238 from the Robert A. Welch Foundation and NIH Grants RR08961 and GM45579.

[‡] The nucleotide sequence(s) reported in this paper has been submitted to the GenBank/EMBL Data Bank under Accession Number AF032389.

* To whom correspondence should be addressed.

[§] Present address: Department of Microbiology, University of Groningen, Kerklaan 30, 9751 NN Haren, The Netherlands.

[1] Abbreviations: PK, pyruvate kinase; RMPK, rabbit muscle pyruvate kinase; RKPK, rabbit kidney pyruvate kinase; MWC, Monod−Wyman−Changeux; PCR, polymerase chain reaction; bp, base pair; IPTG, isopropyl β-D-thiogalactoside; PEP, phosphoenolpyruvate; Phe, L-phenylalanine; FBP, fructose 1,6-bisphosphate; buffer A, 20 mM Tris, 100 mM KCl, 15% (v/v) glycerol, 1 mM dithiothreitol, 0.2 mM fructose 1,6-bisphosphate, 0.1 mM ethylenediaminetetraacetic acid, and 0.1 mM phenylmethanesulfonyl fluoride, pH 7.9; buffer B, 5 mM KP_i, 1 mM ethylenediaminetetraacetic acid, 1 mM dithiothreitol, 0.2 mM fructose 1,6-bisphosphate, 5 mM $MgSO_4$, and 100 mM KCl, pH 7.5; buffer C, same as buffer B at pH 6.0 without KCl; TKM buffer, 50 mM Tris, 72 mM KCl, and 7.2 mM $MgSO_4$, pH 7.5; TK buffer, 50 mM Tris, 72 mM KCl, and 2 mM ethylenediaminetetraacetic acid, pH 7.5; TKMD buffer, 50 mM Tris, 72 mM KCl, 7.2 mM $MgSO_4$, and 0.2 mM dithiothreitol, pH 7.5.

S0006-2960(97)01990-9 CCC: $15.00
Published on Web 02/13/1998

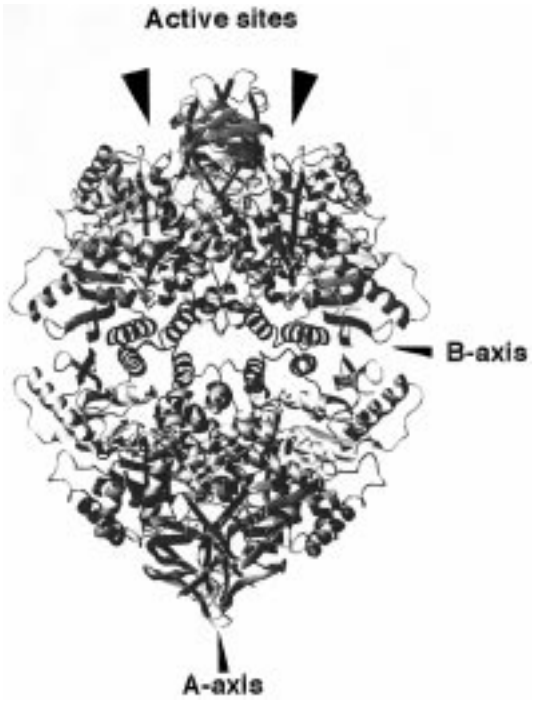

FIGURE 1: Structure of the tetrameric RMPK. The helix−loop−helix regions that are different between the muscle and kidney isozymes are located along the *B*-axis. This subunit interface is positioned away from the active sites. The structure is generated using the coordinates of Larsen et al. (*34*).

PK is widely distributed throughout the body and is the major isozyme derived from kidney and leukocytes. Each isozymic form exhibits distinct kinetic properties to accommodate the various metabolic requirements demanded by the different tissues. In the absence of inhibitor, the muscle and kidney-type PKs exhibit hyperbolic and sigmoidal steady-state kinetic behavior, respectively, and are regulated by a host of allosteric inhibitors and activators (*4*). The physiological rationale for the different isozymes is that the kidney-type isozyme is evolved to permit gluconeogenesis, during which PK activity should be decreased. The muscle-type isozyme is less sensitive to allosteric effectors, which reflects the predominance of glycolysis over gluconeogenesis in muscle. Hence, studying the same regulatory enzyme from different tissues is most likely to provide information for relating a change in regulatory pattern to a change in protein structure that confers the special regulatory features to the enzyme.

(B) The muscle and kidney-type isozymes of rat PK are produced from the same gene by alternative RNA splicing (*5*). The alternative splicing results in a primary sequence difference of 22 amino acids, which are located in a region that forms important intersubunit contacts as shown in Figure 1 (*6*). It was proposed that these differences in sequence may determine the characteristic allosteric properties of each isozyme (*5*, *6*). The relatively small number of differences in sequence enhances the chance of identifying the role of each amino acid difference in conferring changes in allosteric behavior.

(C) Preliminary studies on tissue-derived rabbit kidney PK (RKPK) in this lab, employing analytical ultracentrifugation, indicated that RKPK undergoes subunit disassembly in contrast to RMPK, which is a stable tetramer under all native conditions. Several reports describe the effect of FBP on the molecular weight of the kidney-type isozyme derived from Ehrlich ascites tumor cells (*7*) and human kidney (*8*). These results suggest that this isozyme undergoes self-association which is affected by FBP, an allosteric activator. The kidney isozyme therefore has the potential to provide information about the effect of ligands on the energetics of intersubunit interactions.

Recently, RMPK was cloned and expressed in *Escherichia coli* (*9*), making this study of RKPK possible. RKPK was cloned and expressed in *E. coli*. The purified recombinant RKPK allows for extensive kinetic and physical characterization, which was difficult using authentic RKPK with respect to purification yield and purity. Structural and functional properties of recombinant RKPK were characterized, and the effects of ligands on the subunit interaction are described.

EXPERIMENTAL PROCEDURES

Materials. Pyruvate kinase from rabbit muscle, lactate dehydrogenase, disodium salt of ADP, phosphoenolpyruvate, Tris base, and Tris-HCl were purchased from Boehringer Mannheim. Trypsin, reduced nicotinamide adenine dinucleotide (NADH), L-phenylalanine (Phe), potassium chloride, sodium chloride, and phenylmethanesulfonyl fluoride (PMSF) were all obtained from Sigma Biochemicals. Mono- and dibasic potassium phosphate were purchased from Fisher. ^{35}S-dATP was purchased from Amersham Life Science. Oligonucleotides were purchased from Genosys Biotechnologies, Inc.

RNA Extraction and cDNA Synthesis. After homogenization using a Tekmar tissuemizer, the rabbit kidney tissue was extracted by the combined disruptive and protective properties of guanidine thiocyanate and β-mercaptoethanol (*10*). Extraction of mRNA was performed using the PolyATract mRNA isolation system from Promega. cDNA was synthesized using random hexamer primers and avian myeloblastosis virus reverse transcriptase from the 5′-Ampli Finder RACE kit (Clontech).

Cloning and DNA Sequencing. The gene encoding the rabbit kidney PK was amplified by the polymerase chain reaction according to the manufacturer's instructions, using a DNA thermal cycler (Perkin-Elmer Cetus), except that 2.5 units of Pfu DNA polymerase (Stratagene) was used. The sample was subjected to a "hot start" PCR step at 94 °C for 3 min, followed by a temperature-step cycle of 94 °C (1 min), 70 °C (30 s), and 78 °C (105 s) for a total of 30 cycles, followed by a 7 min extension at 72 °C after the final cycle. A set of primers was designed, based on the coding sequences of the recombinant RMPK (rRMPK) (*9*), bearing both the N-terminal (P1, 5′-CTAAGAATTCATGTC-GAAGTCCCACAGTGA-3′) and the C-terminal (P2, 5′-TTCCAATGC ATCGGTGGCACACTACAG-3′) coding regions of the gene flanked by *Eco*RI and *Nsi*I sites, respectively. These primers were used to generate a 1.7 kb PCR fragment containing the entire open reading frame, which was isolated by agarose gel electrophoresis (1.0%) and gel extraction (Qiagen). The isolated PCR-amplified fragment was digested with *Eco*RI and *Nsi*I and subcloned into the multiple cloning site of pKK223-3 (Pharmacia), which was cut with *Eco*RI and *Pst*I followed by dephosphorylation. Recombinant plasmids (pRK-PK) were introduced into *E. coli* JM105 by electroporation (Gene Pulser, Bio-Rad), in a 0.1 cm cuvette at 1.8 kV.

DNA sequencing of double-stranded DNA was performed by the dideoxynucleotide chain-termination method (*11*) using Sequenase version 2.0 (U.S. Biochemical Corp). Oligonucleotides were synthesized to fit the strategy for sequencing as described (*9*). The region containing the difference in sequence between rRMPK and rRKPK was sequenced completely from both directions.

Overexpression of RKPK. *E. coli* JM105 cells containing the plasmid pRK-PK were grown overnight in M9 minimal medium containing 100 μg/mL ampicillin and were inoculated 1/100 (v/v) into NZCYM medium containing 100 μg/mL ampicillin (*12*). Culture was grown at 37 °C until the optical density at 600 nm reached 0.7−1.0, at which point expression was induced by the addition of IPTG to a final concentration of 60 μg/mL. After 12 h of induction, the cells were harvested by centrifugation at 6000 rpm for 20 min in a Sorvall RC-5C centrifuge using a GS-3 rotor.

Protein Purification and Preparation. All purification steps were performed at 4 °C except the SP-Sepharose chromatography, which was performed at room temperature. The cells were resuspended in 10 volumes of buffer A and disrupted with a Piranha Press (Tesla Inc.) set at 9000 psi. An equal volume of buffer A was added to the cell suspension and centrifuged for 1 h at 10 000 rpm in the GSA rotor of a Sorvall RC-5C. A 10% (v/v) poly(ethylenimine) (pH 7.9) solution was added to the supernatant, with stirring, to a final concentration of 0.35%. After being stirred for 5 min, the mixture was centrifuged for 15 min at 6000 rpm in a GSA rotor. Solid ammonium sulfate was added to the supernatant in small portions with stirring to 45% saturation. Stirring was continued for 30 min and the precipitated proteins were removed by centrifugation at 8000 rpm in a GSA rotor for 45 min. The supernatant was brought up to 70% ammonium sulfate saturation with stirring and spun as above. The two chromatographic steps were performed on a FPLC system (Pharmacia Biotech Inc.) employing columns made for this system. The pellet was dissolved in up to 5 mL of buffer B and applied to a HiLoad 16/60 (1.6 cm × 60 cm) Superdex 200 column. Fractions, typically containing more than 95% of the total activity, were pooled and dialyzed against buffer C. The dialyzed sample was applied to a 1 mL HiTrap SP-Sepharose (0.4 cm × 2.5 cm) column and the nonadsorbed proteins were removed by washing the column with 25 column volumes of buffer C. The rRKPK was eluted with a 30 mL linear salt gradient from 0 to 1 M NaCl. The eluted rRKPK was collected, precipitated with 70% ammonium sulfate, and stored at 4 °C.

Recombinant RKPK was desalted before all experiments by filtration using a Superdex-200 AG column on a FPLC system. The ammonium sulfate precipitate was concentrated by centrifugation at 14 000 rpm in an Eppendorf tabletop centrifuge for 5 min and the pellet was resuspended in up to 300 μL of the appropriate buffer before being loaded onto the filtration column. The protein concentration was determined by absorbance at 280 nm, using an absorptivity of 0.54 mL/(mg·cm) (*13*).

Identification of Trypsin Fragments of rRKPK and rRMPK Using High-Performance Liquid Chromatography/Electrospray Mass Spectrometry. For the tryptic digest, 100 μL of 0.6 mg/mL PK in 100 mM ammonium bicarbonate was mixed with 100 μL of 4 M urea in 100 mM ammonium bicarbonate. At an enzyme/substrate ratio of 1:20 (w/w), a 12 h incubation at 37 °C was then performed. The sample was subsequently reduced by 5 mM DTT for 0.5 h, after which time the reaction was quenched by adding 1 mL of a 0.1% (v/v) trifluoroacetic acid (TFA)/H_2O. One hundred and twenty five picomoles of the tryptic digests were used for fragment identification on reversed-phase high-performance liquid chromatography/electrospray mass spectrometry (RP-HPLC/ES-MS).

RP-HPLC/ES-MS was performed using a Rainin HPLC system interfaced to a quadrupole mass spectrometer equipped with a nebulization-assisted electrospray probe (VG Platform, Fisons Instruments, Altrincham, U.K.). No ultraviolet detector was employed. Data were acquired and processed with a Microsoft Windows-based software system (VG MassLynx, Fisons Instruments, Altrincham, U.K.). Lens voltages, resolution settings, calibration method, and instrument configuration were as previously described (*39*).

The RP-HPLC conditions involved gradient elution using two mobile phases: (A) 0.1% (v/v) TFA/H_2O and (B) 0.1% (v/v) TFA/acetonitrile. The run involved a 10-min isocratic period at 1% B followed by a linear 1%/min gradient between 1 and 51% solvent B. The mass spectrometer scanned over a range of 250−2000 in mass-to-charge (m/z) ratio at 10 s/scan with a peak step width of $^1/_{16}$ Da. The source temperature was set at 200 °C.

Enzyme Kinetics. The enzymatic activity of rRKPK was determined by the lactate dehydrogenase-coupled enzyme assay (*14*). The reaction occurs in a solution consisting of 50 mM Tris base, 72 mM KCl, 7.2 mM $MgSO_4$, 0.3 mM NADH, 10 μg/mL lactate dehydrogenase, and varying amount of Phe and FBP as indicated. The final concentration of ADP or PEP in the assay mixture was fixed at 4 or 2 mM, respectively, while the concentration of the other substrate was varied. After the pH of the assay mix was adjusted to 7.5 at 23 °C, LDH that was equilibrated with TKM buffer was added and the assay mix was finally brought to the desired volume. The reaction was started by the addition of 0.12 μg of PK in 3 μL of TKMD to 1 mL of assay solution that had been equilibrated at 23 °C. The decrease in absorption at 340 nm was followed as a function of time with a Hitachi U-2000 spectrophotometer to obtain v, the observed steady-state kinetic velocity. All data sets were fitted to the modified version of Hill equation (*15*)

$$v = \frac{V_{max}[S]^n}{K_{app}{}^n + [S]^n} \quad (1)$$

where V_{max} is the maximal velocity of each data set, [S] is the concentration of the variable substrate, n is the Hill coefficient, and K_{app} is a complex steady-state kinetic equilibrium constant that is equivalent to K_m in the Michaelis−Menten equation where $n = 1$.

SDS−Polyacrylamide Gel Electrophoresis. SDS−10% polyacrylamide gel electrophoresis was performed according to the method of Laemmli (*16*), followed by staining with Coomassie Blue. The markers used for molecular mass determination were phosphorylase *b* (97 400 Da), bovine serum albumin (66 200 Da); ovalbumin (45 000 Da), and carbonic anhydrase (31 000 Da).

Analytical Gel Chromatography. For the analytical gel chromatography experiments a Superdex-200 HR 10/30

```
1     TCGAAGTCCC ACAGTGAAGC CGGGTCTGCC TTCATCCAGA CGCAGCAGCT GCACGCAGCC
      S  K  S  H  S  E  A  G  S  A  F  I  Q  T  Q  Q  L  H  A  A   20
61    ATGGCGGACA CATTCCTGGA GCACATGTGC CGGCTGGACA TCGACTCCGC GCCCATCACG
      M  A  D  T  F  L  E  H  M  C  R  L  D  I  D  S  A  P  I  T   40
121   GCCCGCAACA CGGGCATCAT CTGTACCATC GGCCCTGCCT CCCGATCGGT GGAGACGCTG
      A  R  N  T  G  I  I  C  T  I  G  P  A  S  R  S  V  E  T  L   60
181   AAGGAGATGA TCAAGTCTGG GATGAACGTG GCGCGCATGA ACTTCTCCCA CGGAACTCAC
      K  E  M  I  K  S  G  M  N  V  A  R  M  N  F  S  H  G  T  H   80
241   GAGTACCATG CGGAGACCAT CAAGAACGTG CGCACAGCCA CGGAAAGCTT TGCCTCAGAC
      E  Y  H  A  E  T  I  K  N  V  R  T  A  T  E  S  F  A  S  D  100
301   CCCATCCTCT ACCGGCCCGT CGCGGTGGCT CTGGACACTA AGGGACCCGA GATCCGAACG
      P  I  L  Y  R  P  V  A  V  A  L  D  T  K  G  P  E  I  R  T  120
361   GGGCTCATCA AGGGCAGCGG CACGGCGGAG GTGGAGCTGA AGAAGGGAGC CACGCTCAAG
      G  L  I  K  G  S  G  T  A  E  V  E  L  K  K  G  A  T  L  K  140
421   ATCACGCTGG ACAACGCCTA CATGGAGAAG TGCGACGAGA ACATCCTGTG GCTGGACTAC
      I  T  L  D  N  A  Y  M  E  K  C  D  E  N  I  L  W  L  D  Y  160
481   AAGAACATTT GCAAGGTGGT GGACGTGGGC AGCAAGGTCT ACGTGGACGA CGGCCTCATC
      K  N  I  C  K  V  V  D  V  G  S  K  V  Y  V  D  D  G  L  I  180
541   TCCCTGCAGG TGAAGCAGAA AGGTCCTGAC TTCCTGGTGA CGGAGGTGGA GAACGGTGGC
      S  L  Q  V  K  Q  K  G  P  D  F  L  V  T  E  V  E  N  G  G  200
601   TTCTTGGGCA GCAAGAAGGG CGTGAACCTC CCCGGGGCTG CGGTGGACCT GCCTGCCGTG
      F  L  G  S  K  K  G  V  N  L  P  G  A  A  V  D  L  P  A  V  220
661   TCCGAGAAGG ACATCCAGGA TCTGAAGTTC GGCGTGGAGC AGGACGTGGA CATGGTGTTT
      S  E  K  D  I  Q  D  L  K  F  G  V  E  Q  D  V  D  M  V  F  240
721   GCCTCTTTCA TCCGCAAGGC GGCTGACGTC CATGAGGTCA GGAAGATCCT GGGAGAGAAA
      A  S  F  I  R  K  A  A  D  V  H  E  V  R  K  I  L  G  E  K  260
781   GGGAAGAACA TCAAGATCAT CAGCAAAATT GAGAACCACG AGGGGGTGCG CAGGTTTGAT
      G  K  N  I  K  I  I  S  K  I  E  N  H  E  G  V  R  R  F  D  280
841   GAGATCCTGG AGGCCAGCGA CGGGATCATG GTGGCTCGTG GTGATCTTGG CATTGAGATT
      E  I  L  E  A  S  D  G  I  M  V  A  R  G  D  L  G  I  E  I  300
901   CCTGCAGAGA AGGTCTTCCT TGCCCAGAAG ATGATAATTG GGCGATGCAA CCGTGCTGGG
      P  A  E  K  V  F  L  A  Q  K  M  I  I  G  R  C  N  R  A  G  320
961   AAGCCTGTCA TCTGTGCCAC GCAGATGCTG GAGAGCATGA TCAAGAAGCC CCGCCCCACC
      K  P  V  I  C  A  T  Q  M  L  E  S  M  I  K  K  P  R  P  T  340
1021  CGCGCCGAGG GCAGTGACGT GGCCAACGCG GTCCTGGATG GAGCCGACTG CATCATGCTG
      R  A  E  G  S  D  V  A  N  A  V  L  D  G  A  D  C  I  M  L  360
1081  TCTGGAGAGA CGGCCAAGGG CGACTACCCG CTGGAGGCCG TCCGCATGCA GCACCTGATT
      S  G  E  T  A  K  G  D  Y  P  L  E  A  V  R  M  Q  H  L  I  380
1141  GCCCGTGAGG CAGAGGCTGC CATCTACCAC TTGCAATTAT TTGAGGAGCT CCGCCGCCTG
      A  R  E  A  E  A  A  I  Y  H  L  Q  L  F  E  E  L  R  R  L  400
1201  GCGCCCATTA CCAGCGACCC CACAGAAGCC GCCGCCGTGG GCGCCGTGGA GGCCTCCTTC
      A  P  I  T  S  D  P  T  E  A  A  A  V  G  A  V  E  A  S  F  420
1261  AAGTGCTGCA GTGGGGCCAT AATCGTGCTG ACCAAGTCTG GCAGGTCTGC TCACCAAGTG
      K  C  C  S  G  A  I  I  V  L  T  K  S  G  R  S  A  H  Q  V  440
1321  GCCCGGTACC GCCCGCGCGC CCCCATCATT GCCGTGACAC GGAACCACCA GACCGCCCGC
      A  R  Y  R  P  R  A  P  I  I  A  V  T  R  N  H  Q  T  A  R  460
1381  CAGGCCCACC TGTACCGTGG GATCTTCCCG GTGGTGTGTA AGGATCCGGT CCAGGAGGCC
      Q  A  H  L  Y  R  G  I  F  P  V  V  C  K  D  P  V  Q  E  A  480
1441  TGGGCTGAGG ATGTCGACCT CCGGGTGAAC TTGGCCATGA ATGTCGGCAA GGCCCGCGGT
      W  A  E  D  V  D  L  R  V  N  L  A  M  N  V  G  K  A  R  G  500
1501  TTCTTCAAGA AGGGAGATGT GGTCATTGTG CTCACCGGAT GGCGCCCTGG CTCTGGCTTC
      F  F  K  K  G  D  V  V  I  V  L  T  G  W  R  P  G  S  G  F  520
1561  ACCAACACCA TGCGCGTGGT GCCCGTGCCG TGA
      T  N  T  M  R  V  V  P  V  P  STOP
```

FIGURE 2: Nucleotide and deduced amino acid sequence of RKPK. The predicted amino acid sequence is shown by the single-letter code under the nucleotide sequence, and numbers are indicated on the right for the amino acids and on the left for the nucleotides. Bases and amino acids diverging from the sequence of RMPK (*9*) are doubly underlined. Peptide fragments not verified by mass spectrometry are singly underlined.

Table 1: Purification of RKPK from *E. coli* (1L)

	total protein (mg)	total activity (units)	recovery (%)	specific activity (units/mg)
cell-free extract after centrifugation	208	683	100	3.3
after 0.3% poly(ethylenimine) precipitation	39	440	64	11.3
45−70% $(NH_4)_2SO_4$ pellet	22	488	71	22.2
superdex−200HL chromatography	10.2	362	53	53.3
SP−Sepharose chromatography	1.2	217	32	180.8
Superdex−200HR chromatography	0.8	180	26	225.0

column and FPLC (Pharmacia, Uppsala, Sweden) were employed. The column was equilibrated with TKMD at room temperature, with or without a ligand, and 100 μL rRKPK samples were loaded onto the column. Fractions (0.5 mL) were collected and PK activity was measured using the method described above. The following proteins were used for column calibration: catalase (240 000 Da), aldolase (158 000 Da), and albumin (66 200 Da) (calibration proteins II for gel chromatography, Combithek, Boehringer Mannheim GmbH).

Circular Dichroism. CD spectra of rRKPK and rRMPK were measured with an Aviv 62 DS circular dichroism spectropolarimeter. Solutions of 0.6 and 0.13 mg/mL were measured in a fused quartz cuvette with a path length of 0.1 cm. The 0.04 mg/mL samples were measured in a fused quartz cuvette with a path length of 1 cm. Each spectrum was recorded with a 0.5 nm increment and 1 s interval from 260 to 190 nm. For each sample three repetitive scans were obtained and averaged.

Velocity Sedimentation. Velocity sedimentation experiments were performed in a Beckman Optima XL-A analytical ultracentrifuge (Palo Alto, CA) equipped with absorption optics. The experiments were carried out at 30 000 rpm at 23 °C with an An-60Ti rotor, and data were collected at 230 or 280 nm in the continuous mode with a radial step size of 0.003 cm, at 8 min intervals. Weight-average sedimentation coefficients were obtained by employing the Beckman data analysis software.

RESULTS

Cloning and Nucleotide Sequencing of rRKPK. The rat muscle and kidney-type PK isozymes are produced from the same gene by alternative RNA splicing (*5*). Since the alternative exon is not located at the ends of the PK coding sequence, a set of primers was designed according to the coding sequence of the rabbit muscle PK. These primers were used to amplify a DNA fragment by PCR, resulting in a 1.7 kilobase pair fragment that has the size and restriction pattern expected for RKPK.

Since the cloned RKPK gene is a result of a PCR amplification, alterations in the sequence might have been introduced. If indeed this were the case, variation in DNA sequences from different clones would be expected. However, identical nucleotide sequence was observed from two clones and is summarized in Figure 2. Hence, it may be concluded that in this case PCR amplification did not result in any alteration in the sequence. The open reading frame of 1593 bp runs from the ATG start codon to a TGA stop codon, with a deduced protein sequence of 530 amino acids. The nucleotide sequence also revealed that the *Eco*RI restriction site flanking the RMPK gene was cloned into the *Eco*RI site of pKK223-3 next to the putative Shine−Dalgarno sequence with the correct orientation.

The nucleotide sequence of rRKPK is identical to the nucleotide sequence of rRMPK (*9*) except for short sequences within the 1140−1294 region. This region corresponds well with the location of the alternative exons observed in rat PK isozymes (*5*), which code for amino acids 380−435.

Overexpression and Purification of RKPK. Only the *E. coli* that contained pRK-PK showed an IPTG-inducible protein as indicated by a band observed by SDS−PAGE. This IPTG-inducible band has a slightly lower electrophoretic mobility than authentic RMPK isolated directly from rabbit muscle, which is characteristic for kidney PK (*17*).

Purification of rRKPK from *E. coli* was performed by a procedure that is identical to that for rRMPK, except that 0.2 mM FBP and 1 mM DTT were included in the buffers. In the absence of a reducing agent the activity of rRKPK disappears within hours. The addition of FBP during KPK purification has been reported (*18*). The purified recombinant RKPK was about 95% homogeneous according to a densitometric analysis of the SDS−polyacrylamide gel. The results of a typical purification process for 1 L of culture are summarized in Table 1.

Recombinant RKPK activity is not as stable as that of rRMPK. Therefore, it is essential to carry through the purification method promptly. Generally, the sample should be in buffer C within 10 h after cell disruption. The rRKPK, stored in ammonium sulfate, is desalted by a filtration column (see Materials and Methods). This step serves two purposes. First, buffer exchange is fast and complete. Second, purity of the rRKPK sample is further improved (Table 1).

Peptide Mapping of rRKPK and rRMPK. Peptide mapping employing RP-HPLC/ES-MS is an accurate and effective method to verify primary sequences. A 125 pmol aliquot of a tryptic digest of rRKPK or rRMPK was separated by RP-HPLC, on-line with a ES-MS analyzing over the range of 250−2000 *m*/*z*. Each separated fragment produces a series of multiple-charged ions on a mass-to-charge (*m*/*z*) ratio scale. On this scale, the positions of the multiple-charged positive ions from a single fragment of molecular weight M_r are given by

$$m/z = (M_r + nH)/n \qquad (2)$$

where H is the mass of the proton and n is a series of consecutive integers (*19*). Data were acquired, processed, and analyzed with the MassLynx software. The software assigned a peptide code to each tryptic fragment starting from the N-terminus and assuming that the tryptic digestion was complete. Both rRKPK and rRMPK have the same number of tryptic fragments. As listed in column 1, Table 2, a total of 63 fragments are expected. The corresponding residue numbers are listed in column 2, Table 2. On the basis of the sequence similarity and difference between rRKPK and rRMPK, the peptide fragments expected in each isozyme are

Table 2: Identification of Tryptic Fragments of RKPK and RMPK with RP HPLC/ES MS

peptide code	residues	expected K/M[a]	found K/M[a]	*R*t (min) K/M[a]	theoretical mass (av)[b]	observed mass ± SD[c] K/M[a,d]	charged species K/M
T21	186−187	+/+	−/−	−/−	274.32	−/−	−/−
T50	433−435	+/−	+/−	24.72/−	318.33	318.41 ± 0.00/−	1/−
T32	263−265	+/+	−/+	−/8.27	373.45	−/373.76 ± 0.00	−/1
T9	89−91	+/+	+/+	19.18/19.07	387.44	387.62 ± 0.00/388.33 ± 0.00	1/1
T40	316−318	+/+	+/−	39.26/−	391.45	390.81 ± 0.00/−	1/−
T33	266−269	+/+	+/+	22.42/22.63	459.59	459.53 ± 0.00/460.05 ± 0.00	1/1
T18	162−165	+/+	+/+	25.33/25.69	476.60	476.46 ± 0.00/476.96 ± 0.00	1/1
T15	136−140	+/+	+/+	21.68/21.95	488.58	488.68 ± 0.00/488.89 ± 0.00	1/1
T60	500−503	+/+	+/+	40.38/40.26	497.59	497.72 ± 0.00/498.05 ± 0.00	1/1
T63	526−530	+/+	+/+	35.81/36.01	509.65	509.70 ± 0.00/510.03 ± 0.00	1/1
T6	62−65	+/+	+/+	27.06/27.48	519.66	520.14 ± 0.44/520.69 ± 0.56	1,2/1,2
T12	120−124	+/+	+/+	32.35/32.69	530.67	530.80 ± 0.10/531.12 ± 0.12	1,2/1,2
T30	256−260	+/+	+/+	31.23/31.50	558.68	558.24 ± 0.80/559.14 ± 0.29	1,2/1,2
T11	115−119	+/+	+/+	26.35/26.71	570.65	570.86 ± 0.08/570.53 ± 0.41	1,2/1,2
T39	311−315	+/+	+/+	34.89/35.15	588.77	588.92 ± 0.44/589.81 ± 0.0*	1,2/1
T52	443−446	+/+	+/+	22.62/22.97	590.68	591.03 ± 0.62/591.27 ± 0.59	1,2/1,2
T5	56−61	+/+	+/+	29.0/29.29	675.78	675.84 ± 0.26/676.72 ± 0.77	1,2/1,2
T19	166−172	+/+	+/+	25.84/26.20	702.81	702.76 ± 0.20/703.90 ± 0.86	1,2/1,2
T38	305−310	+/+	+/+	35.70/35.49	704.87	705.74 ± 0.00*/705.04 ± 0.00	1/1
T54	455−460	+/+	+/+	41.80/41.44	725.76	724.44 ± 0.28/724.95 ± 0.00	1,2/1
T25	224−229	+/+	+/+	32.25/32.52	730.82	730.38 ± 0.31/730.82 ± 0.00	1,2/1
T7	66−72	+/+	+/+	27.77/27.82	733.85	733.42 ± 0.10/734.06 ± 0.30	1,2/1,2
T42	336−341	+/+	+/+	20.14/20.54	753.90	754.47 ± 0.76/754.71 ± 0.80	1,2,3/1,2
T51	436−442	+/+	+/+	20.85/21.20	767.84	767.38 ± 0.27/768 ± 1.06*	1,2,3/1,2
T55	461−466	+/+	+/+	30.31/30.48	786.89	788.12 ± 0.50/787.86 ± 0.00*	1,2,3/1
T53	447−454	+/+	+/+	39.67/38.39	840.03	840.18 ± 0.47/840.50 ± 0.56	1,2/1,2,3
T56	467−474	+/+	+/−	49.94/−	862.10	862.25 ± 0.68/−	1,2/−
T45	376−382	+/+	+/−	34.99/−	868.07	867.81 ± 0.51/−	1,2,3/−
T48	393−399	−/+	−/+	−/43.91	877.01	−/876.66 ± 0.00	−/1
T28	247−254	+/+	+/+	26.35/26.84	895.97	896.22 ± 0.56/896.42 ± 2.10*	1,2/1,2
T58	489−497	+/+	+/+	39.16/38.81	945.15	945.01 ± 0.56/945.01 ± 0.46	1,2/1,2
T34	270−277	+/+	+/+	25.33/25.69	953.02	952.60 ± 0.32/953.20 ± 0.72	1,2/1,2
T13	125−134	+/+	+/+	32.96/33.11	990.08	990.16 ± 0.44/990.15 ± 0.55	1,2/1,2
T44	367−375	+/+	+/+	35.81/41.10	1019.12	1019.09 ± 0.32/1019.19 ± 0.64*	1,2/1,2
T46	383−391	−/+	−/+	−/32.69	1061.19	−/1062.00 ± 0.00	−/2
T49	422−432	+/−	+/−	46.88/−	1107.40	1108.21 ± 1.69*/−	1,2/−
T37	294−304	+/+	+/+	26.35/26.71	1141.29	1141.56 ± 0.00/1141.89 ± 0.00	2/2
T3	32−42	+/+	+/+	41.60/41.02	1171.32	1171.28 ± 0.52/1171.37 ± 0.94	1,2,3,4/1,2
T16	141−150	+/+	+/+	41.91/41.27	1197.38	1196.86 ± 0.35/1197.57 ± 0.00	1,2/2
T4	43−55	+/+	+/−	44.24/−	1302.52	1302.02 ± 0.23/−	1.2/−
T17	151−161	+/+	−/+	−/43.48	1411.60	−/1411.06 ± 0.16	−/1,2
T50	422−435	−/+	−/+	−/55.36	1416.71	−/1415.13 ± 0.00	−/2
T20	173−185	+/+	+/+	52.18/50.62	1448.68	1448.56 ± 0.07/1448.47 ± 0.33	1,2/1,2
T24	207−223	+/+	+/+	48.21/46.89	1636.87	1636.60 ± 0.07/1636.31 ± 0.24	1,2/1,2
T57	475−488	+/+	+/−	39.06/−	1642.74	1641.96 ± 0.69/−	2,3,4/−
T36	279−293	+/+	+/−	52.58/−	1665.89	1665.72 ± 0.60/−	1,2,3/−
T41	319−335	+/+	+/−	62.71/−	1820.27	1819.29 ± 0.34/−	2,3/−
T26	230−245	+/+	−/+	−/51.48	1860.12	−/1860.70 ± 0.21	−/2,3
T22	188−205	+/+	+/+	59.35/56.81	1866.06	1866.60 ± 0.59/1865.97 ± 0.00	2,3/2
T8	73−88	+/+	+/+	37.12/37.11	1902.08	1900.56 ± 0.00*/1901.08 ± 0.00*	4/4
T46	383−398	+/−	+/−	45.77/−	1932.16	1932.20 ± 0.00*/−	2/−
T48	400−421	+/−	+/−	56.04/−	2145.40	2145.19 ± 0.44/−	2,3/−
T62	505−525	+/+	−/−	−/−	2263.61	−/−	−/−
T49	400−421	−/+	−/+	−/43.14	2303.58	−/2301.82 ± 0.07	−/2,3
T43	342−366	+/+	+/−	60.98/−	2437.69	2437.31 ± 0.32/−	2,3/−
T10	92−114	+/+	+/+	50.54/48.84	2465.79	2464.56 ± 0.00*/2463.84 ± 0.00*	3/3
T2	3−31	+/+	+/−	56.04/−	3218.60	3217.13 ± 0.00	3/−

[a] K and M represent rRKPK and rRMPK fragments, respectively. + and − represent found or expected and not found or expected, respectively. [b] Average mass based on nucleotide sequence of rRKPK (Figure 2) and/or rRMPK (*9*), respectively. [c] Observed masses as determined by automated matching, of expected mass spectral fragment ions with observed ions, by the MassLynx software with parameters set to default values. Standard deviation was calculated only for peptides with more than one observed species. [d] Spectral fragment ions not matched by the MassLynx software but matched by manual evolution on the basis of peak abundance, retention time, and/or the presence of multiply-charged species are indicated by an asterisk.

listed in column 3. Fragments T46, T48, T49, and T50 are expected to be different while the rest of them are expected to be observed in samples from both isozymes. The software converted the deduced amino acid sequences into expected ion masses as listed in column 6. Column 4 lists the 54 fragments that were experimentally observed in each sample. The undetected fragments are those with *m*/*z* ratios of less than 250, the lower limit of range set for this ES-MS analysis. The software matched the expected ion masses, including the multiple-charged species, to the observed masses as listed in column 7. Matching was performed by employing default settings for the targeting parameters. This resulted in the

verification of 78% and 56%, within the mass range analyzed, of the amino acid sequence of rRKPK and rRMPK, respectively. Multiple-charged ions in combination with RP-HPLC unresolved tryptic fragments, incomplete proteolysis, cation adduction and sample heterogeneity can result in complex electrospray spectra, which hampers the verification of some peptides. It is common to observe a peak corresponding to an expected tryptic peptide that appears to yield only a doubly charged ion because the triply charged species is weak or falls on or near a low mass background peak (*20*). These phenomena could explain the detection of a smaller than expected number of charged species (column 8, Table 2).

Fragments not automatically detected by MassLynx were often identifiable by manual evaluation of the chromatograms. Using the *m*/*z* search feature of the BioLynx component of the MassLynx software, the *m*/*z* values for the predicted fragments were entered by hand to generate single-ion chromatograms. The presence of co-eluting, multiply charged peaks, predicted for a given fragment, as well as relative peak area within a series being similar to those obtained for the same proteolytic fragment identified in the other digest, were used as the criteria for manual assignment of peaks. For example, fragment T51 was identified in rRKPK by the MassLynx software but not in the rRMPK sample. However, peaks of similar retention time on the HPLC column were observed in both rRMPK and rRKPK, as shown in column 5. In the mass spectrometer results, the abundance of the singly and doubly charged peaks was similar to the ones observed for the same charged species in rRKPK. Thus, the combination of retention time, abundances and the number of charged species aided in the identification of this fragment in rRMPK. In summary, within the mass range analyzed, inclusion of the manually verified fragments results in a verification of 90 and 68% of the amino acid sequences from rRKPK and rRMPK, respectively. The primary sequence differences between rRKPK and rRMPK were verified by this method since the expected peptides T46, T48, T49, and T50 for both isozymes were verified.

Based on the deduced amino acids, the average molecular weight of rRKPK is 57 774. ES MS analysis of undigested rRKPK resulted in a molecular weight of 57 782 ± 27, which confirms the deduced amino acid sequence of rRKPK.

Kinetic Characterization of rRKPK. Steady-state kinetics of rRKPK as a function of effectors, with PEP as a variable substrate, are shown in Figure 3. Parameters derived from these steady-state kinetics are summarized in Table 3. In the absence of Phe, a plot of the velocity versus substrate concentration was sigmoidal, which indicates a cooperativity between the PEP binding sites. In the presence of the inhibitor Phe, the curve for velocity vs substrate is shifted to the right with a concomitant increase in K_{app}. This shift is more pronounced with increasing Phe concentration, as shown in Figure 3B. The effects of Phe could be reversed by the addition of 10 μM FBP, resulting in a Hill coefficient and K_{app} value smaller than those in the absence of effectors. The K_{app} for ADP, while the concentration of PEP was fixed at 10 mM, was 0.22 ± 0.015 mM. These kinetic behaviors are similar to those reported for kidney PK (*4*, *21*).

Sedimentation Velocity. The quaternary structure of rRKPK was monitored by sedimentation velocity. Weight-average sedimentation coefficients of rRKPK were determined within the protein concentration range of 0.025−1.85 mg/mL at pH 7.5 and 23 °C in TKMD buffer. The weight-average sedimentation coefficient is a function of the protein concentration as depicted in Figure 4. At higher protein concentration the weight-average sedimentation coefficient converges to a value similar to that obtained for the tetrameric rRMPK (*9*). Extrapolation of a double-reciprocal plot of the average sedimentation coefficient vs concentration to infinite concentration yielded a value of 10.50 S for the largest aggregating species. It is more difficult to define the smallest aggregating species since the absorption optics of the analytical ultracentrifuge places a limit of approximately 25 μg/mL. Therefore, the highest associating unit is determined to be a tetramer, but the smallest associating unit can either be a monomer or a dimer. For an associating system, the weight-average sedimentation coefficient is a function of protein concentration as indicated by

$$\bar{S} = \sum S_i^{\circ}(1 - g_i C)\, K_i C_1^{\,i} / \sum K_i C_1^{\,i} \qquad (3)$$

where S_i° is the sedimentation coefficient of the *i*th species extrapolated to infinite dilution, g_i is the respective hydro-

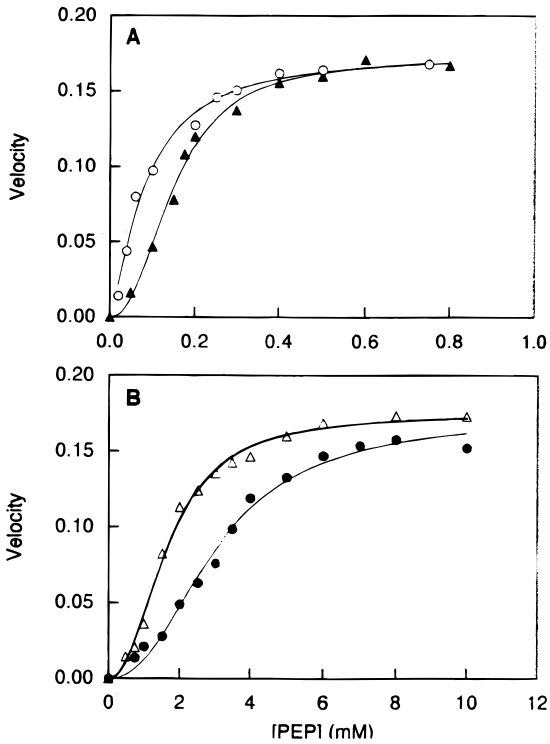

FIGURE 3: Kinetic characterization of rRKPK: PK activity as a function of PEP concentration in the absence (▲) and presence (△) of 1 mM Phe, in the presence of 2 mM Phe (●), and in the presence of 2 mM Phe and 10 μM FBP (○). The lines through the data sets are the result of nonlinear fitting to eq 1. The kinetic parameters resulting from the fittings are shown in Table 3.

Table 3: Kinetic Parameters of RKPK as a Function of Effectors and PEP as the Variable Substrate

	k_{cat}	K_{app} (mM)	n
RKPK	200 ± 2	0.156 ± 0.005	2.1 ± 0.2
RKPK + 1 mM Phe	195 ± 4	1.67 ± 0.006	2.2 ± 0.2
RKPK ± 2 mM Phe	192 ± 9	3.03 ± 0.2	2.3 ± 0.2
RKPK + 2 mM Phe + 10 μM FBP	191 ± 3	0.078 ± 0.005	1.5 ± 0.1

Table 4: Least-Squares Fitting of Weight-Average Sedimentation Velocity Data to Different Modes of Association

model	mode of association	n^a	$S°_{20,w}$	K_n (mL/mg)$^{n-1}$	SSR[b]
I	4M-T	4	4.16, 10.50	99.85 ± 6.92	1.10
II	2D-T	2	6.61, 10.50	27.61 ± 2.96	2.32
III	4M-2D-T	2, 4	4.16, 6.61, 10.50	4.54 ± 4.48, 4806 ± 88.22	1.35

[a] Stoichiometry. [b] The sum of the squares of residuals.

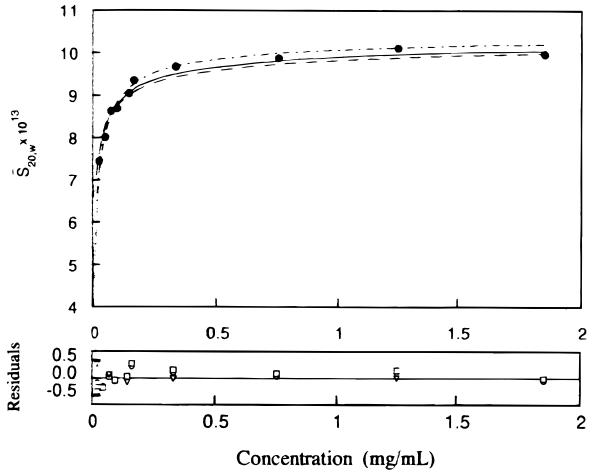

FIGURE 4: Weight-average sedimentation coefficients ($\bar{S}_{20,w}$) of rRKPK as a function of total protein concentration in TKMD buffer at 23 °C. The lines are least-squares fitting to the experimental data according to the models described in Table 4: model I (—), model II (---), and model III (-·-). Residuals are plotted as the observed values minus the calculated values according to model I (○), model II (□), and model III (▽).

dynamic nonideality coefficient, $C = \Sigma K_i C_1^i$, and K_i is the Adair association constant between monomer and any *i*meric species present in solution. K_1 is equal to unity, by definition.

The sedimentation data were analyzed using a nonlinear least-squares curve-fitting procedure previously adopted in this laboratory (*22*−*25*). The fitting procedure requires an input on the values for $S_i°$, which is related by

$$S_i° = S_1°(i)^{2/3}$$

where $S_1°$ is the sedimentation coefficient of the smallest unit undergoing self-assembly. The calculated values are $S_1 = 4.16$ S, $S_2 = 6.61$ S, and $S_4 = 10.5$ S, assuming spherical symmetry for all species (*26, 27*). Every reasonable model was tested. These models include a variety of two-state models and sequential polymerization. The results of the least-squares fittings are summarized in Table 4. As shown in Figure 4, the experimental data fit equally well to the different models. Hence, the mode of association could not be defined using this approach alone. Each data point in Figure 4 corresponds to the weight-average sedimentation coefficient of a reacting system in rapid dynamic equilibrium, which is accurately described by the velocity of the square root of the second moment of the sedimenting boundary (*28*). Extracting only the weight-average sedimentation coefficient of the primary data can result in the loss of valuable information. The shape of the sedimenting boundary can be very diagnostic for detecting the mode of association according to the Gilbert theory (*29*−*31*). The Gilbert theory predicts a single sedimenting peak for macromolecular dimerization ($n = 2$), and for higher order polymerization reactions ($n \geq 3$) the reaction boundary should resolve into two peaks. The appearance of bimodality in the higher-order polymerization reaction is a function of the association constants and the total macromolecular concentration in the plateau region.

Comparing a simulated sedimentation pattern with an experimental sedimentation pattern can be diagnostic for supporting a model describing a self-association equilibrium, particularly when the presence of bimodality is not so obvious (*32*). Sedimentation velocity profiles were simulated on the basis of a method developed by Cox (*33*) and adopted in this laboratory (*25, 31*). The simulated profiles describe a derivative of a sedimentation boundary at a fixed sedimentation time and solute concentration, employing the fitted association constant and values of $S_{20,w}$ for the respective models in Table 4.

Model I fits the $S_{20,w}$ vs C data in Figure 4 to a monomer-tertramer mode of association. The simulated sedimentation profiles for two different protein loading concentrations are shown in Figure 5A. Since the stoichiometry of polymer formation is 4 ($n = 4$), bimodality shown in the simulated data in Figure 5A is consistent with the Gilbert theory. Model II fits the $S_{20,w}$ vs C data in Figure 4 to a dimer−tetramer mode of association for two different protein loading concentrations (Figure 5B). The simulated sedimentation patterns exhibit single sedimenting peaks as predicted by the Gilbert theory for a macromolecular dimerization ($n = 2$). Simulation based on model III resulted in sedimentation patterns similar to those from model I (not shown).

Derivatives of experimental sedimentation patterns, at the protein loading concentrations and sedimentation times used in the simulations, are plotted in Figure 5C. It is evident that the experimental data resemble Figure 5B the best. Therefore, it can be concluded that the mode of association is most likely dimer to tetramer with an equilibrium constant of 28 ± 3 mL/mg.

Analytical Gel Chromatography. Analytical gel chromatography was used to monitor changes in molecular size of the multiple forms of rRKPK, under different conditions. The elution profile of rRKPK is dependent on protein concentration in contrast to rRMPK, as shown in Figure 6A. The shape of the elution profile reflects the presence of the macromolecular species in equilibrium. Under these conditions rRMPK is a stable tetramer; therefore, the shape of the elution profile represents the elution of a single macromolecular species. At a concentration of 6.45 mg/mL rRKPK, the elution profile is identical to that of rRMPK with respect to the shape and the elution volume. This indicates that the highest associating unit is a tetramer, a conclusion consistent with that of the sedimentation data. The elution profile of a 165-fold diluted sample is much broader in shape and it has a significantly higher elution volume, as shown in Figure 6A. At an even lower rRKPK concentration of 4 μg/mL, the width of the elution profile is

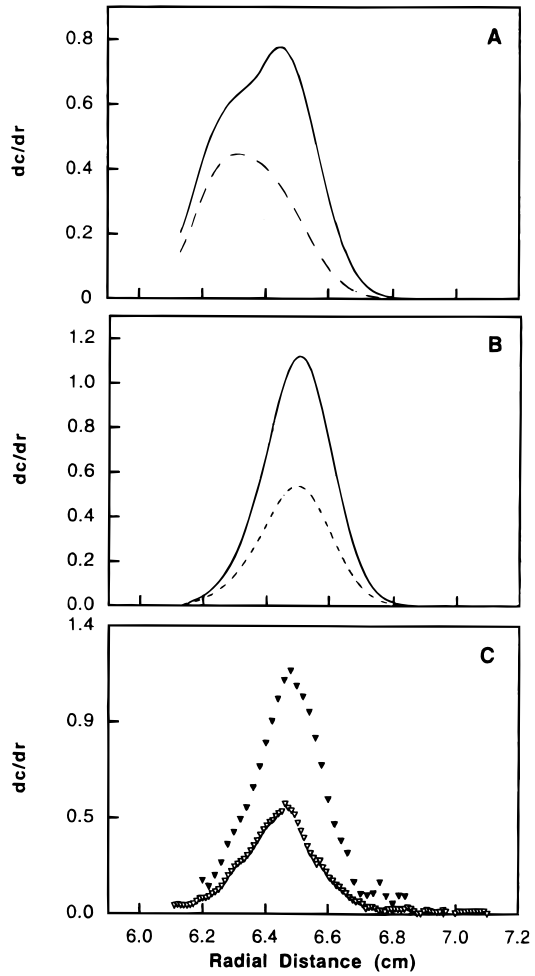

FIGURE 5: Simulated sedimentation velocity patterns of rRKPK at 0.17 mg/mL (---, sedimentation time of 9359 s) and 0.34 mg/mL (—, sedimentation time of 9203 s). A sharp initial boundary was set at 6.1 cm. The ordinate is the concentration gradient in milligrams per milliliter per centimeter, and the abscissa is the radial position in centimeters from the center of rotation. Simulation to model I of Table 4 is shown in panel A and to model II of Table 4 is shown in panel B. Panel C represents the experimental derivatives of sedimentation patterns at 0.17 (▽) and 0.34 mg/mL (▼) rRKPK, after sedimentation times of 9359 and 9203 s, respectively.

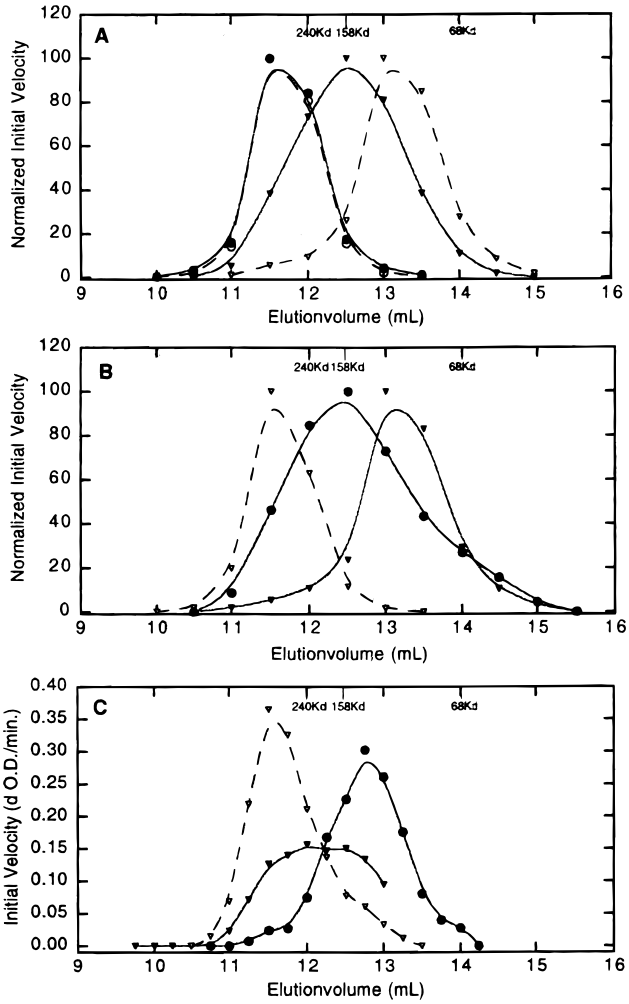

FIGURE 6: Effects of ligands on the elution profile of rRKPK. (A) rRKPK at 6.45 mg/mL (●), 38.7 μg/mL (▼), and 3.9 μg/mL (▽); rRMPK at 11.7 μg/mL (○). (B) rRKPK (18.7 μg/mL) in the presence of 2 mM Phe (▼) or 1 mM FBP (●); rRMPK in the absence of effectors (---). (C) rRKPK (52 μg/mL) in the absence of effectors (▼) or in the presence of 8 mM PEP (▽) or in the presence of 2 mM ADP (●). The lines through the data are drawn to indicate the trend of the data.

narrower and similar to that of rRMPK, implying that at this protein concentration this elution profile represents the presence of a unique species instead of a mixture of interacting species. According to the column calibration the smallest associating form is a dimer. These results indicate that rRKPK undergoes self-association and that the mode of association is dimer to tetramer.

The effects of Phe and FBP, allosteric inhibitor and activator, respectively, on the self-association of rRKPK are shown in Figure 6B. Phe shifts the equilibrium toward the dimer and FBP has the opposite effect. In the presence of PEP the equilibrium is shifted to the tetramer. Interestingly, the presence of the other substrate, ADP, has the opposite effect and shifts the equilibrium toward the dimer, as shown in Figure 6C.

Circular Dichroism. The secondary structure of rRKPK as a function of protein concentrations was monitored by CD and the results are shown in Figure 7. From the analytical gel chromatography and sedimentation velocity

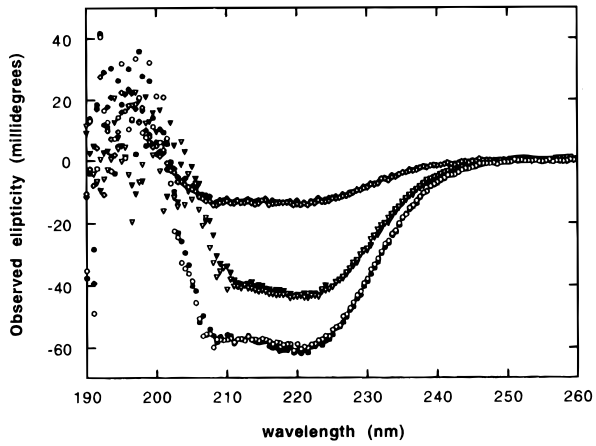

FIGURE 7: CD spectra in the far-UV region of rRKPK and rRMPK as a function of protein concentration: Recombinant RKPK at 0.04 mg/mL (▼), 0.13 mg/mL (■), and 0.6 mg/mL (●) and recombinant RMPK at 0.04 mg/mL (▽), 0.13 mg/mL (□), and 0.6 mg/mL (○).

experiments it is apparent that rRKPK undergoes self-association whereas rRMPK is a stable tetramer. At a protein

concentration of 0.6 mg/mL both isozymes are tetrameric and the CD data indicate no difference in secondary structure. As the protein concentration is decreased to 0.13 and 0.04 mg/mL, the distribution toward dimeric species of rRKPK is increasingly favored by the chemical equilibrium, whereas rRMPK remains a tetramer. The CD spectra of rRKPK at the lower protein concentrations are indistinguishable from that of rRMPK, indicating that there is no detectable change in the secondary structure of rRKPK upon dissociating to a dimer and the structure is not different from that of rRMPK at the same concentrations.

DISCUSSION

The pair of kidney and muscle PK isozymes provides an excellent opportunity to elucidate the molecular mechanism in conferring allostery in an enzyme because of the differences in kinetic and structural properties associated with these isozymes. The muscle isozyme exhibits nonallosteric kinetic behavior while the kidney isozyme demonstrates a full spectrum of allosteric properties under the same experimental conditions. The successful cloning and overexpression of both isozymes places this enzyme system in a favorable position for identifying the roles of the 22 amino acid differences in altering the regulatory behavior of PK. The propensity of kidney PK to undergo subunit assembly and disassembly enables one to monitor the interfacial communications induced by the binding of effectors and substrates. It is now feasible to address questions: Do all effectors and substrates communicate through this particular subunit interface? What is the thermodynamic signature associated with binding of each specific ligand?

Since a difference in only 22 amino acids can apparently exert a significant change in the allosteric behavior and the ultimate goal of this work is to elucidate the roles played by these amino acids in conferring allostery, it is imperative that the primary sequences of rRKPK and rRMPK be determined and verified by multiple approaches. In addition to DNA sequencing, the primary sequences of these isozymes were verified by peptide mapping in combination with mass spectrometry. This method resulted in the verification of 90% and 68% of the rRKPK and rRMPK sequences, respectively. All peptide fragments of the intersubunit region, containing sequence differences between rRKPK and rRMPK, were verified. As a result of the high sequence homology between rRKPK and rRMPK the tryptic digests share many identical peptide fragments. Since these two isozymes are the product of the same gene by alternative RNA splicing, common fragments verified in one isozyme can be used as a verification of that fragment in the other isozyme. On the basis of this assumption, 96% of the sequences from rRKPK and rRMPK are verified, because only peptide fragments T21 and T62 were not found in either sample of digestion. Verification of peptide fragments T26 and T48 by mass spectrometry has additional significance. It confirms the sequence reported by Cheng et al. (*9*), which was different from that reported (*34*). On the basis of the reported differences in sequences, the expected differences in mass for those fragments are 13 and 16. The high accuracy of ES-MS analysis is expected to distinguish those differences in mass in these fragments. The ES-MS analysis of undigested rRKPK provides additional conformation of the deduced primary sequence of rRKPK. The source of the difference in sequence remains obscure. It could be the result of a difference in genetic pool.

The primary structures of the two isozymes differ in 22 positions localized in a helix−loop−helix motif of the C domain that constitutes a major intersubunit contact. This small local sequence difference is responsible for the distinctly different kinetic properties of these two isozymes of PK. To analyze the importance of these 22 residues on the allosteric mechanism, the amino acids at the corresponding 22 positions of the other allosteric PK isozymes were compared with that in the nonallosteric muscle PK isozyme (*35*). Eighteen of the total 19 sequence differences between the allosteric rat erythrocyte and liver PK isozymes and the nonallosteric rabbit muscle PK are at the same positions as the sequence differences between rabbit muscle and kidney PK isozymes. These observations suggest that the sequence differences at the intersubunit contact regions play important roles in mediating the allosteric properties and that the structural elements involved are similar for all isozymes.

The demonstration of the propensity of rRKPK to undergo reversible subunit assembly and disassembly is an important observation. One can take advantage of the thermodynamic linkage between ligand binding and subunit assembly to probe the pathways of intersubunit communication. Sedimentation velocity does not provide enough data to establish unequivocally the mode of association. Since the assembly to tetramer is highly favored, the UV absorption optics of the analytical ultracentrifuge do not enable one to obtain data at sufficiently low protein concentration to establish the identity of the smallest assembly PK species. Nevertheless, analytical gel chromatography provides the needed information to establish that at protein concentrations approaching that in enzyme assay solutions rRKPK exists as a dimer with no indication of further dissociation into monomers under these experimental conditions. Thus, the chromatographic results in addition to the comparison of simulated and experimental sedimentation patterns establishes the mode of PK association as dimer $\rightleftharpoons$ tetramer with an equilibrium constant of 28 ± 3 mL/mg. In all the quantitative analysis of data, it was assumed that the system was in rapid reversible equilibrium. The validity of this assumption is supported by the observation that the value of $\bar{S}$ at a fixed concentration of protein is not a function of angular velocity. The CD data indicate that no detectable change in secondary structure is associated with a change in quaternary structure.

Having defined the mode of association, it is important to take advantage of this physical property to probe the pathway of intersubunit communication. The assembly to tetrameric rRKPK is favored by the binding of PEP, one of the two substrates, or FBP, an activator. In contrast, binding of ADP, the other substrate, shifts the equilibrium toward dimeric rRKPK. A similar situation is observed for Phe, the inhibitor. These semiquantitative observations provide significant new insights into the molecular mechanism of allosteric regulation in the PK system. First, all substrates and effectors communicate through this particular dimer−dimer interface. Second, the thermodynamic signatures of these communications are qualitatively different even for the two substrates, with ADP weakening and PEP strengthening the interaction along this dimer interface. Activator, FBP, and allosteric inhibitor, Phe, exhibit the same pattern of opposing effects on the energetics of dimerization.

Although, as a result of a series of indepth studies, it was shown that the allosteric mechanism of RMPK can be best described by a MWC model, in which the R- and T-states have differential affinity for different ligands, no information is available to indicate the specific intersubunit interfaces through which the ligands elicit their effects (*36*, *37*). This study shows that these ligands, be they substrate or allosteric effector, communicate through, at least, this subunit interface. Furthermore, although these ligands have different binding sites probably located in different parts of the subunit, these sites are all linked to this interface. It is not surprising that the thermodynamic signature for FBP is different from that of Phe because they have opposite functions and effects on the kinetic properties of PK. It is to be expected that their messages are different as reflected by the opposite effects on the energetics of dimer−dimer interaction. However, it is most surprising to observe that the thermodynamic signatures of the two substrates are not only quantitatively but qualitatively different. Yet, if one considers the steady-state kinetic behavior of these two substrates, results of these physical studies may provide a means to probe the mechanism that leads to the steady-state kinetic behavior. Both RMPK[2] and RKPK[3] exhibit substrate antagonism phenomena; i.e., the apparent K_m value of a substrate increases with increasing concentration of the second substrate. Substrate antagonism has the appearance of a substrate behaving like an inhibitor. Thus, it would be consistent to observe different thermodynamic signatures for PEP and ADP. These ligands convey different messages, although both of them are substrates. The qualitative effects of the ligands on the self-association of rRKPK can be viewed in the context of the same MWC model derived for RMPK (*21*). FBP and PEP have a higher affinity for the R-state, thereby favoring the active state of the enzyme. Both of these ligands favor the tetrameric form of rRKPK. ADP and Phe on the other hand, display a higher affinity for the T-state, thereby favoring the less active form of the enzyme. Interestingly, ADP and Phe both favor the dimeric form of rRKPK. Therefore, the qualitative effects of these ligands on subunit self-association parallel the effects of the ligands on the kinetic behavior of rRKPK and RMPK as predicted by the MWC model. Within the context of the alternate conformational states of the MWC model it can be hypothesized that the energetics at the subunit interface are different for the R- and T-states. The shift in the equilibrium between the tetramer and dimer of rRKPK could then reflect the shift in equilibrium between the R- and T-states, respectively, as a result of the differential affinity of the ligands for these alternate states.

Studying subunit self-assembly does not only provide insights on pathway of intersubunit communication and nature of signal elicited by each ligand. It is possible to identify a mechanism for the difference in stability between rRMPK and rRKPK. The specific activity of dilute rRKPK (∼50 μg/mL) decreases after several hours, whereas higher concentrations (1 mg/mL) are stable for at least several days. This inactivation can only partially be reversed by a reducing agent. In the absence of reducing agent, activity disappears within hours and oxidation appears to favor the dimeric form. rRKPK can also be stabilized by FBP, which favors the formation of the tetrameric form of rRKPK. These results indicate that the tetrameric form of rRKPK is more stable and the stabilizing effects of DTT, high protein concentration, and FBP are the consequences of shifting the dimer−tetramer equilibrium in favor of the tetramer, which is the quaternary structure of the stable rRMPK.

Results of this study establish rRKPK as an ideal system to define the linkages among subunit assembly, ligand binding, conformational change, and catalytic efficiency. Consequently, this laboratory is defining these linkages in a similar fashion as in the human hemoglobin system (*38*) to probe the ground rules of allosteric regulation in PK.

[2] S. Fredricksen et al., manuscript in preparation.
[3] H. Pan et al., manuscript in preparation.

ACKNOWLEDGMENT

A critical review of the manuscript by Dr. Hong Pan and preparation of Figure 1 by Dr. John Wooll are greatly appreciated. Thanks to Prof. R. Fox for making the mass spectrometer available.

REFERENCES

1. Monod, J., Wyman, J., and Changeux, J. D. (1965) *J. Mol. Biol. 12*, 88−118.
2. Koshland, D. E., Nenethy, G., and Filmer, D. (1996) *Biochemistry 5*, 365−385.
3. Perutz, M. F. (1990) *Mechanisms of Cooperativity and Allosteric Regulation in Proteins*, Cambridge University Press, Cambridge, U.K.
4. Hall, E. R., and Cottam, G. L. (1978) *Int. J. Biochem. 9*, 785−793.
5. Noguchi, T., Inoue, H., and Tanaka, T. (1986) *J. Biol. Chem. 261*, 13807−13812.
6. Murihead, H., Clayden, D. A., Bradford, D., Lorimer, C. G., Fothergill-Gilmore, L. A., Schiltz, E., and Schmidt, W. (1986) *EMBO J. 5*, 475−481.
7. Sparmann, G., Schultz, J., and Hofmann, E. (1973) *FEBS Lett. 36*, 305−308.
8. Harkins, R. N., Black, J. A., and Rittenberg, M. B. (1977) *Biochemistry 16*, 3831−3837.
9. Cheng, X., Friesen, R. H. E., and Lee, J. C. (1996) *J. Biol. Chem. 271*, 6313−6321.
10. Chirgwin, J. M., Przybyla, A. E., MacDonald, R. J., and Rutter, W. J. (1979) *Biochemistry 18*, 5294−5299.
11. Sanger, F., Nicklen, S., and Coulson, A. R. (1977) *Proc. Natl. Acad. Sci. U.S.A. 74*, 5463−5467.
12. Sambrook, J., Fritsch, E. F., and Maniatis, T. (1989) *Molecular Cloning: A Laboratory Manual*, 2nd ed., Cold Spring Harbor Laboratory Press, Cold Spring Harbor, NY.
13. Boyer, P. D. (1962) in *The Enzymes* (Boyer, P. D., Lardy, H., and Myrback, K., Eds.) Vol. 6, pp 95−113, Academic Press, New York.
14. Bucher, T., and Pfleiderer, G. (1955) *Methods Enzymol. 1*, 435−440.
15. Hill, A. V. (1910) *J. Physiol. 40*, 190−224.
16. Laemmli, U.K. (1970) *Nature 227*, 680−685.
17. Saheki, S., Saheki, K., and Tanaka, T. (1982) *Biochim. Biophys. Acta 704*, 484−493.
18. Harada, K., Saheki, S., Wada, K., and Tanaka, T. (1978) *Biochim. Biophys. Acta 524*, 327−339.
19. Fenn, J. B., Mann, M., Meng, C. K., Wong, S. F., and Whitehouse, C. M. (1989) *Science 240*, 64−71.
20. Hemling, M. E., Roberts, G. D., Johnson, W., and Carr, S. A. (1990) *Biomed. Environ. Mass Spectrosc. 19*, 677−691.
21. Consler, T. G., Woodard, S. H.; Lee, J. C. (1989) *Biochemistry 28*, 8756−8764.
22. Hesterberg, L. K., and Lee, J. C. (1981) *Biochemistry 20*, 2974−2980.
23. Hesterberg, L. K., and Lee, J. C. (1982) *Biochemistry 21*, 216−222.

24. Callaci, T. P., Cai, G. Z., Lee, J. C., Daly, T. J., and Wu, C. W. (1990) *Biochemistry 34*, 8752−8762.
25. Harris, S., Williams, R. C., and Lee, J. C. (1995) *Biochemistry 34*, 8752−8762.
26. Cann, J. R. (1970) *Interacting Macromolecules: Theory and Practice of their Electrophoresis, Ultracentrifugation and Chromatography*, Academic Press, New York.
27. Nichol, L. W., Bethune, J. L., Kegeles, G., and Hess, E. L. (1964) In *The Proteins, 2nd Ed.* (Neurath, H., Ed.) pp 305−403, Academic Press, New York.
28. Schachman, H. K. (1959) *Ultracentrifugation in Biochemistry*, Academic Press, New York.
29. Gilbert, G. A. (1955) *Discuss. Faraday Soc. 20*, 68−71.
30. Gilbert, G. A. (1959) *Proc. R. Soc. A250*, 377−388.
31. Lee, J. C., and Surendran, R. (1994) in *Modern Analytical Ultracentrifugation: Acquisition and Interpretation of Data for Biological and Synthetic Polymer Systems* (Schuster, T. M., and Laue, T. M. Eds.) pp 138−155, Birkhauer, Boston.
32. Gilbert, L. M., and Gilbert, G. A. (1973) *Methods Enzymol. 27*, 273−296.
33. Cox, D. J. (1971) *Arch. Biochem. Biophys. 119*, 514−526.
34. Larsen, T. M., Laughlin, T., Holden, H. M., Rayment, I., and Reed, G. H. (1994) *Biochemistry 33*, 6301−6309.
35. Fothergill-Gilmore, L. A., and Michels, P. A. M. (1992) *Prog. Biophys. Mol. Biol. 59*, 105−235.
36. Oberfelder, R. W., Lee, L.-Y., and Lee, J. C. (1984a) *Biochemistry 23*, 3813−3821.
37. Oberfelder, R. W., Barisas, B. G., and Lee, J. C. (1984b) *Biochemistry 23*, 3822−3826.
38. Holt, J. M., and Ackers, G. K. (1995) *FASEB J. 9*, 210−218.
39. Ledman, D. W., and Fox, R. O. (1997) *J. Am. Soc. Mass Spectrom. 8*, 1158−1164.

BI971990C